RESEARCH OF A LATERAL REAMER BIT FOR DIGGING PLANTING HOLE IN ROCKY ABANDONED MINE AREA
/
面向废弃矿山地区造林挖坑的横向扩孔钻具研究

Luo Haifeng *), Chen Chaoyu
Beijing Forest University, Beijing / China;
Tel: 8601062338144; E-mail: luohaifeng@bjfu.edu.cn
DOI: https://doi.org/10.35633/inmateh-65-13

Keywords: *rock, planting hole, lateral, reamer bit, metamorphic, digging*

ABSTRACT
In the abandoned mine area with Karst landform in China, soils are few and thin but rocks are common, traditional planting hole diggers are unequal to work in rocks for vegetation restoration. A reamer bit with variable lateral drilling radius was designed based on the PDC (polycrystalline diamond compact) bit technology and metamorphic mechanism. Two lateral camber blades with PDC teeth were installed inside the bit body, a screw mechanism was employed as the actuation and a spatial double triangle mechanism was taken for the transmission. The curve of the camber blade was specially defined thus the reaming load was decentralized to 85.7% teeth on the blade. The kinematics of the lateral reamer bit was analysed, the mapping models from the actuation to the reaming radius and speed were established. Concrete samples were reamed indoors from 240mm to 407mm in diameter, the reaming cutting load and time length were measured and analysed. The lateral reamer bit was approved with the experiment results, this study provided equipment support for digging the planting hole in rocky abandoned mine areas and also expanded the PDC bit application.

摘要
中国岩溶地区废弃矿山缺乏土壤岩石大面积裸露，传统植树挖坑机无法在岩石中挖坑造林，生态恢复难度大，亟需研制岩石钻孔挖坑机。结合岩石 PDC 钻头技术及变胞机构理论，设计了横向可变钻削半径的扩孔钻头。钻头内对称布置了 2 个镶 PDC 齿的横向曲面刀翼，以螺旋传动机构为变径驱动，以空间双三角形机构为传动机构，为均衡扩孔载荷单独定义了曲面刀翼形状。分析建立了横向扩孔钻头的运动学模型，推导了驱动螺旋到输出扩孔半径及速度的映射模型。以混凝土试样为对象，进行了室内横向240mm至407mm直径的扩孔试验，测试分析了扩孔过程中的载荷曲线及时间。验证了横向岩石内部扩孔挖坑的可行性,本文的研究为岩溶地区废弃矿山的挖坑造林提供了装备支持，同时扩大了PDC 钻具技术的应用场景。

INTRODUCTION

The abandoned mines affect and even destroy the regional ecosystem, making the ecological restoration of abandoned mine area an inevitable step of social civilization (*Zhang J.D. et al., 2020*). The abandoned mine in southwest China, combined with the landform of Karst stony desertification, brings serious challenge in vegetation restoration and commercial crop growing (*Dai Q.H. et al., 2018*). The soil layer is thin and few, whereas the rocks of big area are common, and the heavy rainfall washes the soil away yearly. The planting hole for vegetation, forestry sapling even fruit tree in this rocky area is not feasible to be dug by the traditional digging mechanism (*Yoshida T. et al., 2013*), as the rock is quite different with soil in material behaviour such as hardness and strength. The hole inside the rocks are drilled mostly by the PDC bit, which has a market share of about 85% (*Scott D., 2015*), the digging mechanism for the planting hole in rocky abandoned mine area is thus supposed to be constructed as a PDC bit type. The PDC bit for rocks is often with two or more blades, and the PDC teeth (shorten as tooth and teeth in the following text) are welded along the edge of the blades in a manner that all the teeth can cut the rock material one by one when the bit rotates and feeds forward. The shape and diameter of the holes made in the rock are directly determined by the bit blades and teeth on them, the existing blades on the bit are mostly fixed structure. The hole is thus a single straight cylinder shape with a constant diameter, which is equal to the cutting dimension of the bit teeth (*Tang Q.Q. et al., 2018; Wang S.N. et al., 2014; Yang Y.X. et al., 2019*). The hole in rock can be reamed by another bigger size bit which is installed behind the guiding bit, in the axis direction of hole and extends a long depth (*Sun R.J. et al., 2017; Yang Y.X. et al., 2020*).

Another type of drill bit for foundation stake in the civil engineering of rocky area is basically constructed with a metamorphic triangle blades, the hole with a cone shape for the stake is reamed by the teeth on the hypotenuse of triangle blades (*Hu Z.H., 2020*). The existing digging mechanism and PDC bit found in the literature are not competent in digging the planting hole directly in the rocky abandoned mine area.

A lateral reamer bit for digging the planting hole in rocky abandoned mine area was designed based on the PDC bit technology (*Huang Z.Q. et al, 2017*) and metamorphic mechanism (*Wang R.G. et al., 2019*), the blade of the reamer bit was evolved from traditional type (*Akbari et al, 2016*) to a camber shape. The curve of the blade was studied mainly with two relevant angles, a spatial double triangle mechanism was employed as the transmission mechanism for turning the blades. The resistance cutting load of the reamer bit were tested indoors with a lateral reamer bit prototype and concrete samples.

MATERIALS AND METHODS

Materials

In the rocky abandoned mine area with Karst landform, the soil is precious to grow vegetation, and it is more possible to be washed away by the heavy rainfall. The expected planting hole is preferred to have a big intra-rock space but a small neck channel to protect the soil from losing, as shown in Figure 1, which has an improved shape compared with the common planting hole in the rich soil area. The intra-rock planting hole is also able to contain more soil to improve survival rate of the sapling for forestry or even fruit tree. The variable diameters of the neck channel and intra-rock space demand a metamorphic structure for the new PDC digging bit (*Wang R.G. et al., 2019*). The new bit is expected to drill a hole with small diameter inside the rock first, and later ream the small hole to an intra-rock space, as indicated in Figure 1.

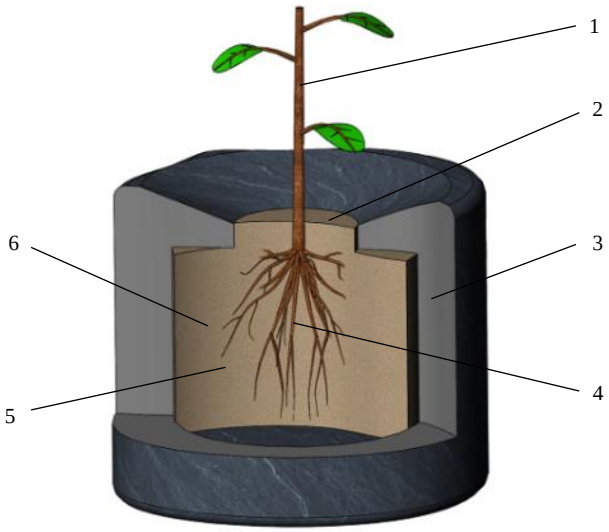

Fig. 1 - Planting hole in rock

1. Sapling; 2. Neck channel; 3. Rock; 4. Root; 5. Soil; 6. Intra-rock space

Methods

Mechanical structure of the reamer bit

To dig the intra-rock planting hole, the drill bit is expected to dig a straight hole of small diameter, and later the small hole is reamed laterally to a big space. The first step can be done by the existing drill bit without difficulty, the second step is the research target in this study. Figure 2. a shows the mechanical structure of the lateral reamer bit for digging the intra-rock planting hole. Two symmetrical camber blades are installed inside the main body via rotation joints R shown in Figure 2. c, the teeth are welded on the external surface of the camber blades to cut the side material of the small inner hole. The internal distal of the camber blade is drove with an universal joint pin (cross axis B and B'), which is further motivated by the upper push bar and lower push bar at joint B. The upper push bar and lower push bar are vertically connected to the upper slider and lower slider through joints A and C, which are further drove by the push rod and pull rod, the push rod and pull rod are linked to a screw joint D outside the guide column. The fixed handle is attached to the push rod, the drive handle and fixed handle are the actuation components to drive the screw joint D and following parts to unfold or withdraw the camber blades relative to the main body.

The transmission of a single lateral reamer bit is simplified and shown as Figure 2. b and c, the actuation triangle ΔABC is comprised of upper push bar (l_{AB}) and lower push bar (l_{BC}, $l_{AB}=l_{BC}$) at the side view, joints A and C are with a distance r_0 to the main body axis O and are drove symmetrically by the screw joint D. And the height h of the triangle ΔABC is the virtual part that actuates the camber blade through the universal joint B' at the top view. The unfolding triangle $\Delta ORB'$ for the camber blade is formed by OR (l_{OR}, structure distance of joint R to axis O), RB'($l_{RB'}$, structure distance of joint R to joint B') and OB' ($l_{OB'}$, distance of joint O to joint B', $l_{OB'}=h+r_0$). The displacement of joint A and C are labelled as s_1 and s_2 ($|s_1|=|s_2|$). The final unfolding angle displacement of line RB' at joint R is marked as θ. With the spatial double triangle transmission mechanism, the actuation displacement s_1 from the screw joint D is transformed to the rotation angle θ of the camber blade, the reaming structure and related cutting radius of the reamer bit is thus varied and controlled.

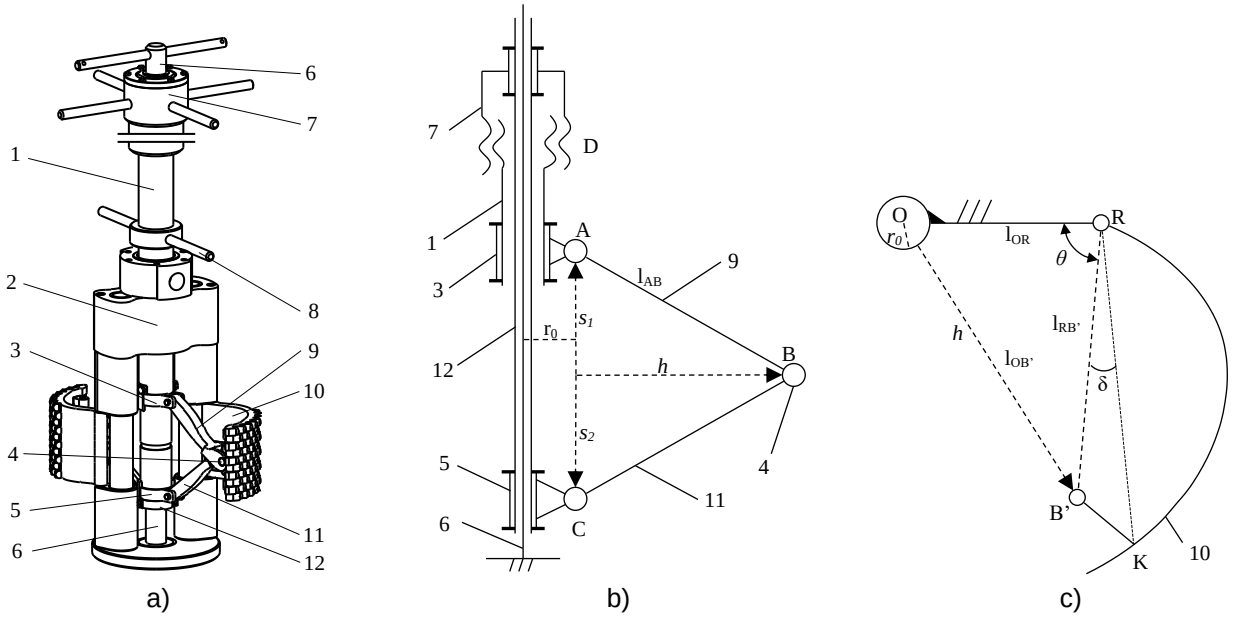

a) b) c)

Fig. 2 - Metamorphic lateral reamer bit

a) Mechanical structure; b) Actuation triangle (side view); c) Unfolding triangle (top view)

1. Push rod; 2. Main body; 3. Upper slider; 4. Universal joint pin; 5. Lower slider; 6. Guide column; 7. Drive handle; 8. Fixed handle; 9. Upper push bar; 10. Camber blade; 11. Lower push bar; 12. Pull rod

With geometric model of the reamer bit shown in Figure 2. b and c, the height h of the actuation triangle ΔABC can be obtained as:

$$h=\sqrt{l_{AB}^2-s_1^2} \tag{1}$$

In the unfolding triangle $\Delta ORB'$ it has:

$$\cos\theta=(l_{OR}^2+l_{RB'}^2-l_{OB'}^2)/2l_{OR}l_{RB'} \tag{2}$$

And the unfolding joint angle θ is thus:

$$\theta=\text{acos}\frac{l_{OR}^2+l_{RB'}^2-(\sqrt{l_{AB}^2-s_1^2}+r_0)^2}{2l_{OR}l_{RB'}} \tag{3}$$

Curve of the camber blade

The teeth are welded on the surface of camber blade, the cutting characteristic of the lateral reamer bit is directly determined by the curve of the camber blade. To decentralize the cutting load averagely to each teeth, the reaming cutting is designed to be started from the proximal tooth to the distal tooth on the camber blade. The curve of the camber blade is defined as following steps as shown in Figure 3. B_i ($i=1,2,\ldots 9$) is the typical point on the camber blade curve RB_i, the tip of teeth T_i is welded and overlap with point B_i.

Step 1: an auxiliary line RK is defined through joint R, with an angle α_0 relative to the minus of OR. A series of concentric arcs with radius of r_i ($r_{i+1} = r_i + 5$) are intersected with line RK at points B_i', B_i' is the reference cutting point of each cutting radius of r_i;

Step 2: at the beginning of the anti-clock wise unfolding for the camber blade curve RB_i, the tooth T_1 on point B_1 is the first one to be rotated out and to cut the material, with the cutting point B_1' on line RK and a radius of r_1. The cutting radius r_i of other teeth T_i on B_i ($i \neq 1$) is less than r_1, the reaming cutting around radius of r_1 is done by the tooth T_1;

Step 3: the curve RB_i is then unfolded with an angle $\angle KRC_1$ ($\angle KRC_1 = \angle C_iRC_{i-1} = \beta$, $i = 2,....9$), the tooth T_2 on point B_2 is rotated to the position B_2' on line RK, the cutting radius is increased to r_2. Tooth T_1 on the position B_1 is rotated to the radial line RC_1, the cutting radius r_i of other teeth T_i ($i \neq 2$) is less than r_2, the reaming cutting around radius of r_2 is done by the tooth T_2;

Step 4: the curve RB_i is unfolded step by step with an angle $\angle KRC_1$, each tooth T_i on point B_i is rotated to the position of B_i' on line RK, the related cutting radius becomes r_i. B_{i-1} is rotated to the radial line RC_{9+1-i}, the cutting radius r_j of other tooth T_j on B_j ($j \neq i$) is less than r_i, the reaming cutting around radius of r_i is done by tooth T_i on point B_i;

Step 5: as the last point B_9 is unfolded to the line RK, the curve RB_i is formed mainly by the points B_i (i=1,2, ...9). The precise position of each B_i can be obtained from above steps.

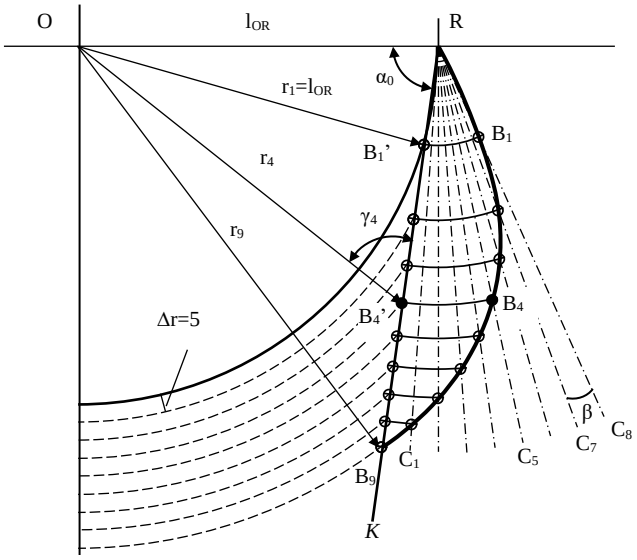

Fig. 3 - Camber blade curve

Take point B_4 as an example, in the triangle $\Delta ORB_4'$ it has:

$$\frac{l_{OR}}{\sin\gamma_4} = \frac{r_4}{\sin\alpha_0} \tag{4}$$

It deduces:

$$\gamma_4 = \text{asin}\frac{l_{OR} \cdot \sin\alpha_0}{r_4} \tag{5}$$

For l_{RB4} of RB_4' in the triangle $\Delta ORB_4'$ it also has:

$$\frac{l_{RB_4'}}{\sin(\pi - \alpha_0 - \gamma_4)} = \frac{r_4}{\sin\alpha_0} \tag{6}$$

Thus:

$$l_{RB_4} = l_{RB_4'} = \frac{r_4 \cdot \sin(\pi - \alpha_0 - \gamma_4)}{\sin\alpha_0} \tag{7}$$

With the l_{RB_4} and $\angle ORC_5=\pi+\pi\cdot(\alpha_0+(9\text{-}4)\cdot\beta)/180$, the present coordination of B_4 are:

$$\begin{cases} x_{B_i}=l_{RB_4}\cdot\cos(\pi+\pi\cdot(\alpha_0+(N\text{-}i)\cdot\beta)/180)+l_{OR} \\ y_{B_i}=l_{RB_4}\cdot\sin(\pi+\pi\cdot(\alpha_0+(N\text{-}i)\cdot\beta)/180) \end{cases},\ N=9, i=4 \tag{8}$$

The position of each point B_i ($i=1,....9$) on the curve RB_i in Figure 3 can be obtained similarly with equation (8), and the shape of the camber blade is thus determined. The curve RB_i is then rotated clock-wise with an angle of $(N-1)\beta$ to withdraw it inside the initial radius of r_1. The coordination of each point B_i can be further deduced when the camber blade is unfolded again with a smaller step angle of $\beta/2$ in the normal reaming process as:

$$\begin{cases} x'_{B_{ij}}=l_{RB_i}\cdot\cos(\pi+\pi\cdot(\alpha_0-(N\text{-}1)\cdot\beta+(N\text{-}i)\cdot\beta+j\cdot\beta/2)/180)+l_{OR} \\ y'_{B_{ij}}=l_{RB_i}\cdot\sin(\pi+\pi\cdot(\alpha_0-(N\text{-}1)\cdot\beta+(N\text{-}i)\cdot\beta+j\cdot\beta/2)/180) \end{cases} \tag{9}$$

Here $N=9$, $i=1...9$, j=1..16, j is the serial number of step unfolding rotation for the camber blade, the cutting radius of each tooth T_i on B_i ($i=2,....9$) relative to the step rotation is thus:

$$r_{cT_{ij}}=\sqrt{(x'_{B_{ij}})^2+(y'_{B_{ij}})^2} \tag{10}$$

And the max cutting radius of the camber blade on each step unfolding rotation is obtained as:

$$r_j(\alpha_0,\beta)=\max r_{cT_{ij}},\ i=1,2...N,\ j=1,2...16 \tag{11}$$

The parameters for camber blade curve RB_i can be further increased to $N=21$, $j=40$, $r_1=100$, $r_{21}=200$, the reaming cutting radius is thus varied from 100mm to 200mm. The instantaneous max reaming cutting radius r_j of each step unfolding rotation is related to a certain tooth T_i, and the relation between r_j and T_i is affected by the angles α_0 and β. The preferred parameters of them are determined as α_0=88° β=3.4° finally to decentralize the cutting load to majority of teeth. And the reaming cutting radius r_j and related tooth number T_i are calculated with equation (10) to (11) and shown in Figure 4. a. Not exactly as expected, the camber blade cuts from tooth T_3 to T_{20} as it is unfolded, it means 85.7% of the teeth are functional in the reaming process, and each tooth T_i cuts about two or three step rotations of $\beta/2$ for the camber blade. The actual simplified camber blade curve and structure in this study is shown in Figure 4. b, 75 teeth are assembled row (7 teeth) by row (8 teeth) on one camber blade totally, to ream the rock hole from 220mm to 400mm in diameter. The back angle of each tooth T_i is set as 12 degrees relative to the curve normal at point B_i to ream with a low resistance load (*Huang Z.Q. et al, 2017*).

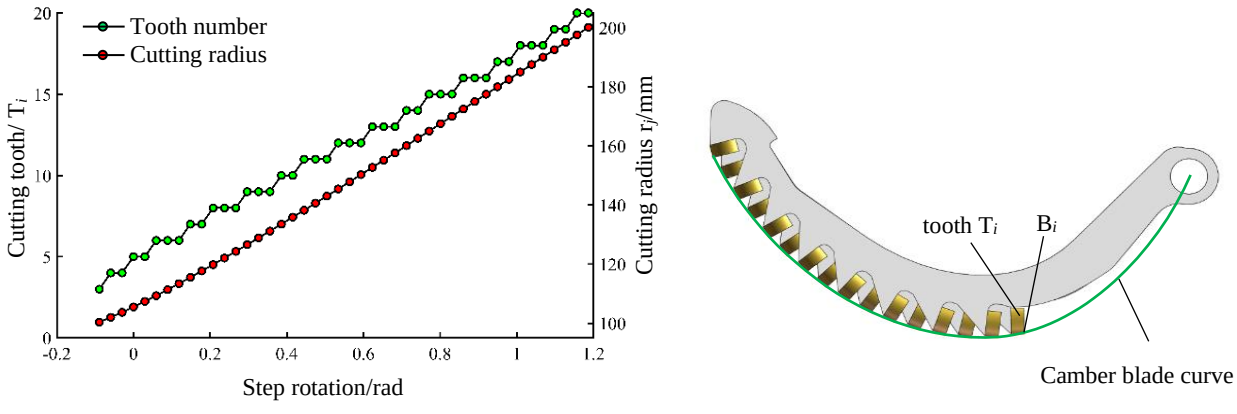

Fig. 4 - Cutting characteristic of camber blade

a) Cutting radius and related tooth; b) Preferred camber blade curve and actual structure

Reaming cutting radius of the reamer bit

Joint the equations (11) and (3), the relation between the displacement s_1 of the actuation triangle ΔABC and the cutting radius r_j of the camber blade is deduced as:

$$r(s_1)=\max\left(\begin{array}{l}\left(\frac{r_i\cdot\sin(\pi-\alpha_0\text{-asin}\gamma_i)}{\sin\alpha_0}\cos(\pi+\pi\cdot\frac{\alpha_0+\delta+\beta\text{-i}\cdot\beta}{180}+\text{acos}\frac{l_{OR}^2+l_{RB'}^2-(\sqrt{l_{AB}^2-s_1^2}+r_0)^2}{2l_{OR}l_{RB'}})+l_{OR}\right)^2\\ +\left(\frac{r_i\cdot\sin(\pi-\alpha_0\text{-asin}\gamma_i)}{\sin\alpha_0}\sin(\pi+\pi\cdot\frac{\alpha_0+\delta+\beta\text{-i}\cdot\beta}{180}+\text{acos}\frac{l_{OR}^2+l_{RB'}^2-(\sqrt{l_{AB}^2-s_1^2}+r_0)^2}{2l_{OR}l_{RB'}})\right)^2\end{array}\right)^{1/2} \quad (12)$$

Where $i=1,2\ldots21,$ and $\delta=2.93^o$ is the structure angle between RB' and auxiliary line RK in Figure 2. c. The variation of reaming cutting radius $r(s_1)$ of the bit is calculated with equation (12) and shown in Figure 5. a. The reaming radius $r(s_1)$ is increased rapidly at the beginning of the actuation displacement (s_0-s_1, s_0 is the original position of s_1), and slows down in the latter process. Differentiating the equation (12) to time t, the reaming speed of the camber blade $v_{r(s_1)}$ can be deduced as:

$$v_{r(s_1)}=\frac{dr(s_1)}{dt}=\frac{dr(s_1)}{ds_1}\cdot\frac{ds_1}{dt}=r'(s_1)\cdot v_{s_1} \quad (13)$$

The $r'(s_1)$ is the derivative of the reamer radius $r(s_1)$ to s_1, which is determined by the transmission parameters of the reamer bit, and the relationship between the actuation speed v_{s_1} and reaming speed $v_{r(s_1)}$ is reflected with it. As the reaming radius $r(s_1)$ is increased with a constant bit rotation speed, the relative speed of the tooth to the rock material will increase linearly. To maintain a constant cutting volume of the rock material in a time period for a tooth, the actuation speed v_{s_1} of the camber blade should be controlled as shown in Figure 5. b. The time length is calculated as about 3 hours, and the expected actuation speed v_{s_1} is increased from about 0.002mm/s to about 0.012 mm/s.

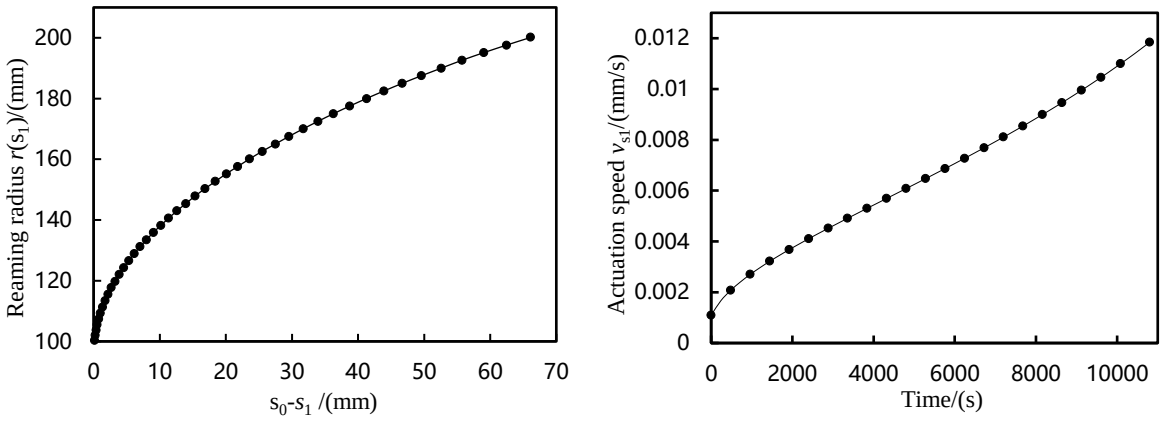

a) b)

Fig. 5 – Reaming radius and actuation speed for camber blade

a) Reaming radius to actuation; b) Expected actuation speed to time

RESULTS

Prototype and indoor experiment

The prototype of the lateral reamer bit has been built and assembled as shown in Figure 6, and the reaming cutting experiments are carried out with it indoors. The max reaming dimension is designed as 400mm in diameter and 130 in height one time to ease the initial test process. The main body of the reamer bit is arranged to be still but the reaming target sample is drove to rotate by motor relative to the bit axis.

The reaming sample is made of concrete with small rocks around 10mm in dimension, as the standard cylindrical rock sample of 450mm in diameter is difficult to get. The concrete sample is rotationally installed on the frame under the reamer bit, four side supporters are arranged around it to improve the rotation precision of the sample, and also to make the concrete sample being coaxial with the reamer bit. The reamer bit is installed on a lifting board, which is drove by manual lift screw mechanism and guided with the guide rail, to land the reamer bit to the inside of the concrete sample. As mentioned above, this study puts emphasis on the reaming process, the concrete sample is constructed as a tubular shape with an inner hole of 240 mm in diameter. The reaming cutting torque of the bit is transformed to the pressure from the measure arm to the pressure sensor on the lift board. A displacement sensor is installed to the fixed handle to measure the motion of the push rod (S_1). A pump circulation system is employed to provide water flow to cool the reaming tooth and take away the drill cuttings made inside the concrete sample.

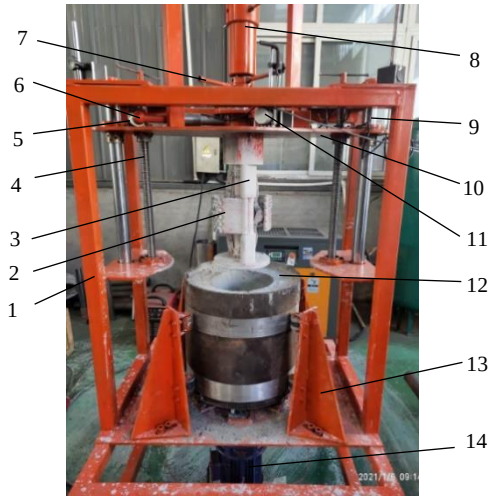

Fig. 6 - Experiment setup for lateral reaming bit

1. Frame; 2. Camber blade; 3. Main body; 4. Lift screw; 5. Pressure sensor; 6. Measure arm; 7. Fixed handle; 8. Drive handle; 9. Guide rail; 10. Lift board; 11. Displacement sensor; 12. Concrete sample; 13. Side supporter; 14. Motor

The parameters of the parts employed in the indoor reaming experiment are listed in Table 1. The experiment was firstly carried out with the concrete sample being rotated at speed of 24 rot/min (*Dai X.W. et al., 2020; Zhu X.H. et al., 2020*), and the initial actuation speed of the screw mechanism for the reaming of the camber blade was set as about 0.001 mm/s, as shown in Figure 5. b. The signals of the pressure sensor and displacement sensor, and the time length for a whole reaming process were both recorded, the speed for rotating the concrete sample was improved for each sample.

Table 1

Parameters of experiment parts

Item	**Inner hole diameter of concrete sample [mm]**	**Diameter of concrete sample [mm]**	**Height of concrete sample [mm]**	**Range of displacement sensor [mm]**	**Precision of displacement sensor [mm]**	**Pump flow [m³/h]**
Parameters	240	450	450	300	0.2	8
Item	**Range of pressure sensor [N]**	**Precision of pressure sensor [N]**	**Power of motor [kW]**	**Speed of motor[rot/min]**	**Reaming height of bit [mm]**	**Min reaming diameter [mm]**
Parameters	1000	1	3	0-60	130	220
Item	**Max reaming diameter[mm]**	**Diameter of tooth [mm]**	**Total number of teeth**	**Back angle of tooth [degree]**	**Strength of concrete sample [MPa]**	**Number of concrete samples**
Parameters	400	13.4	150	12	32	4

Experiment result and analysis

Four concrete samples were reamed in the indoor experiment, and the reaming result of the fourth concrete sample was shown in Figure 7. The concrete sample was constructed with an inner hole of 240mm

in diameter, as shown in Figure 7. a and b, and the inner hole was a little larger than the initial reaming diameter 220mm of the prototype bit to ease the preparation of experiment. The inner hole of the concrete sample was finally reamed to 407mm in diameter, as shown in Figure 7. c. The side face of the reamed hole was cut with corrugated shape, as shown in Figure 7. d and e, the corrugated shape was made by the serried teeth rows on the camber blade. The enlarged view in Figure 7. e for the corrugated side face of the reamed hole indicated that the small rocks in the concrete sample were tightly fixed in the sample without breakage in the reaming process. And the small rocks are reamed layer by layer to the corrugated shape under the reaming cutting of the teeth, the concrete sample was considered to be qualified for the reaming cutting validation. The dimensions of the reamed inner hole in the fourth concrete sample was measured and shown in Figure 7. g, the max diameter of the reamed hole was measured as 407mm, and the height of the reamed hole was 195mm, which was combined with a whole height reaming and a half height reaming of the bit, and the height of the reamed hole could be further increased if the reamer bit was fed more along the height direction by the lift screw mechanism. During the reaming process of the concrete sample, no slag had been generated by the bit, all the materials in the cutting area were transformed to fines and then mixed with water into slurry, as shown in Figure 7. c. The transmission mechanism, camber blades, teeth were in good condition after reaming the four concrete samples, no macroscopic wear was found at the cutting edge of the teeth. As the flow magnitude of the pump was not powerful enough, the bit balling was found on the camber blades, as shown in Figure 7. f, which should be improved in the future.

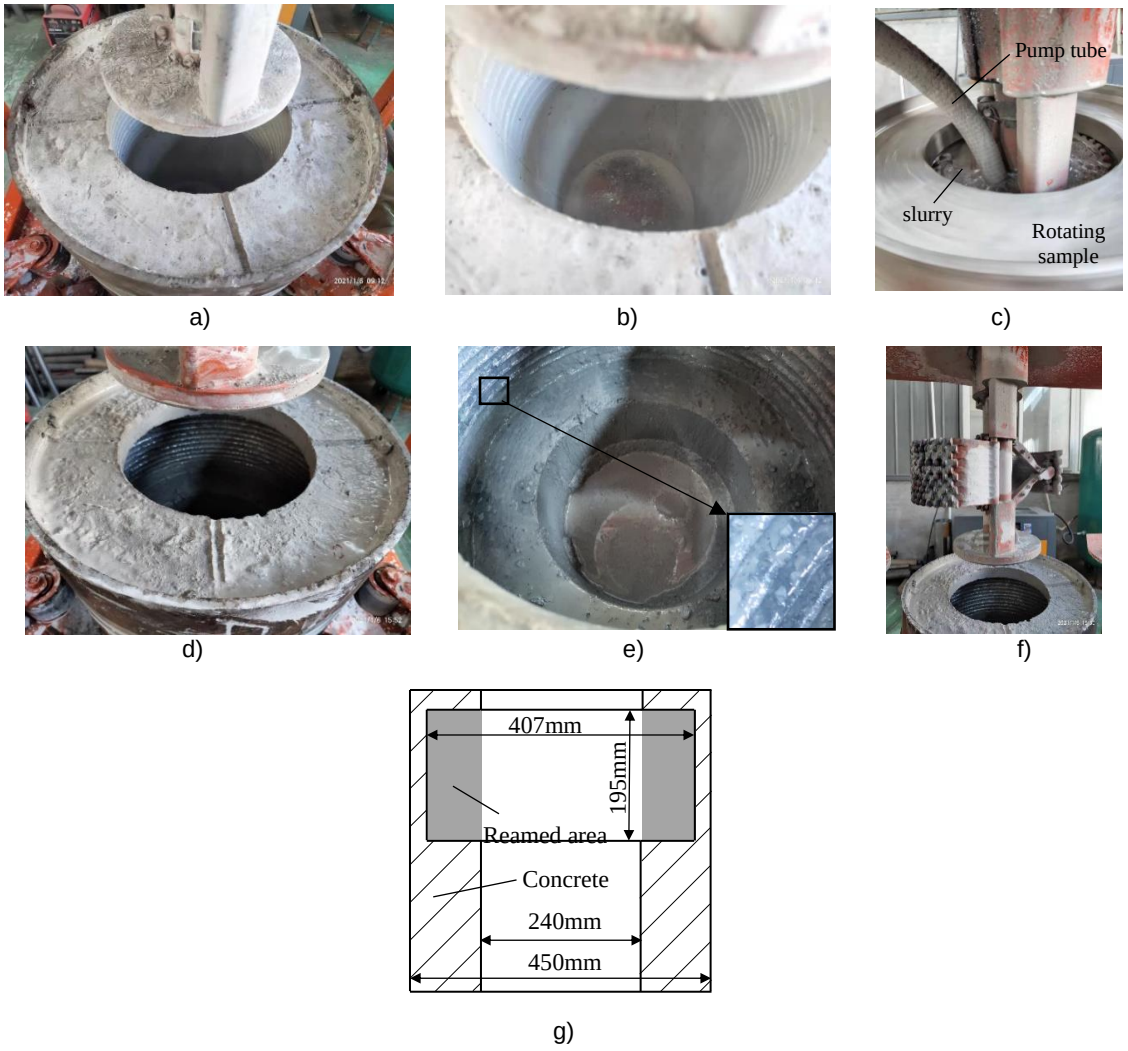

Fig. 7 - Reaming process of concrete sample

a) Sample before reaming; b) Inner hole before reaming; c) Reaming the sample; d) Reamed sample; e) Inside of reamed sample; f) Max reaming radius of the bit; g) Profiles of reamed sample

The displacement of the actuation screw mechanism for reaming the fourth concrete sample was measured and shown in Figure 8. a, the time length was totally about 6000s (1.6h). Due to the material fragility of the concrete sample, the reaming cutting was accompanied by the vibration between the tooth and the concrete sample, the signal of the displacement sensor was disturbed by the vibration of prototype machine,

as the impulse shown on the displacement curve. The actuation speed for the screw mechanism was further calculated with the displacement signals and shown in Figure 8. b, the actual actuation speed was increased from about 0.002 m/s to 0.025 m/s for the fourth concrete sample, it was about two times relative to the curve value in Figure 5. b., which had a similar curve shape but longer time period. The axis speed for the fourth concrete sample was set at about 60 rot/min.

The reaming cutting resistance load for the fourth concrete sample was measured and recorded as shown in Figure 8. c, the resistance torque for single teeth row on the camber blade waved around 10N.m due to the vibration of the reamer bit. The reaming cutting load and time length for reaming the four concrete samples were combined in Figure 8. d. As the rotation speed of the concrete sample was improved from 24rot/min to 36 rot/min, 48 rot/min and 60rot/min, the reaming cutting torque for single teeth row was reduced from about 20.5Nm to 13.3Nm, 11.3Nm and 9.6Nm as expected (*Abugharara et al., 2019; Rostamsowlat et al., 2018*), but the rate for torque decline became smaller. The time length for concrete sample reaming was also reduced from 4.1h to 3h, 2.3h and 1.6h, it was more efficient to ream the rock with higher rotations speed under the circumstances of device safety.

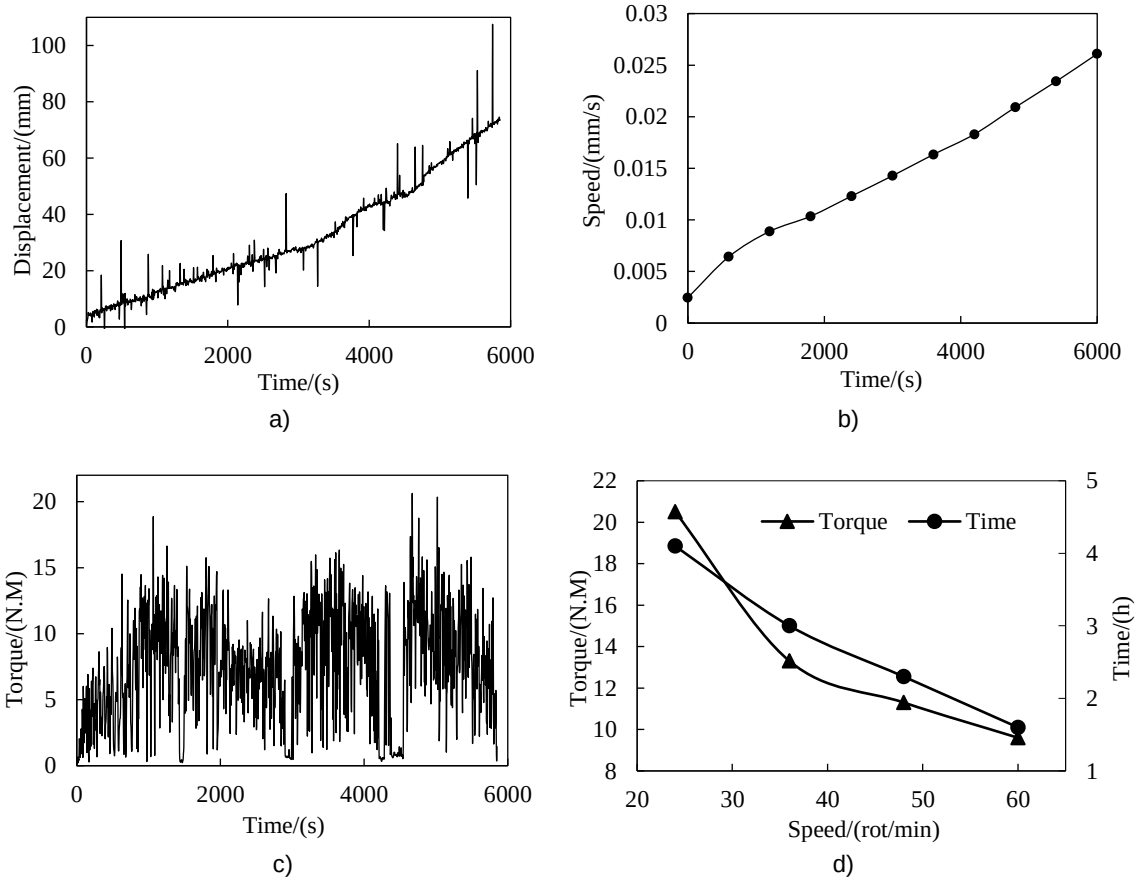

Fig. 8 - Reaming cutting parameters

a) Displacement of actuation; b) Speed of actuation; c) Resistance load; d) Resistance and time to actuation speeds

CONCLUSIONS

(1). To dig the planting hole in the rocky abandoned mine areas, a lateral reamer bit which integrated the PDC bit technology and metamorphic mechanism was proposed in this study. The mechanical structure of the lateral bit was designed mainly with two symmetrical lateral camber blades drove by the spatial double triangle transmission mechanism.

(2). The kinematics model for the transmission mechanism was established, to decentralize the reaming cutting load of the teeth on the camber blade, the curve of blade was defined mainly considering the angle α_0 of the auxiliary line RK and the step rotation angle β of the camber blade.

The preferred parameters were determined as α_0=88° and β=3.4°, with a utilization rate of 85.7% of the teeth on the camber blade. The mapping models from the actuation screw mechanism to the final reaming radius and speed were deduced.

(3). Four concrete samples were employed to test the lateral reamer bit indoors. The inner holes of the concrete samples were reamed from 240mm to 407mm in diameter. The concrete samples were reamed with lower resistance load and shorter time length as the rotation speed of the concrete sample was improved. The experiment result approved the lateral reaming method and bit design, and the planting hole was feasible to be dug with it for the vegetation restoration in abandoned mine area. Improvement is need for the present design of the lateral reamer bit to obtain better reaming cutting effect.

ACKNOWLEDGEMENT

This work is supported by the Fundamental Research Funds for the Central Universities (2017ZY46) and National Science Foundation (Grant numbers: 51705022)

REFERENCES

[1] Akbari B, Miska S. (2016). The effects of chamfer and back rake angle on PDC cutters friction[J]. *Journal of Natural Gas Science and Engineering*, 33, 347-353.

[2] Abugharara A.N, Mohamed B, Hurich C, Molgaard J. (2019). Experimental investigation of the effect of shale anisotropy orientation on the main drilling parameters influencing oriented drilling performance in shale[J]. *Journal of Energy Resources Technology-Transactions of the ASME*, 141(10).

[3] Dai XW, Huang ZW, Shi HZ, Cheng Z. (2020). Rock failure analysis based on the cutting force in the single PDC cutter tests[J]. *Journal of Petroleum Science and Engineering*, 194.

[4] Dai QH, Yan YJ. (2018). Advances in studies on rocky desertification and soil erosion in Karst regions in southwest China [J]. *Journal of Soil and Water Conservation*, 32(02), 1-10.

[5] Hu ZH. (2020). Design and Construction of hydraulic reaming device [J]. *Construction Technology*, 49(01), 48-50.

[6] Huang ZQ, Ma YC, Li Q, Xie D. (2017). Geometry and force modelling, and mechanical properties study of polycrystalline diamond compact bit under wearing condition based on numerical analysis[J]. *Advances in Mechanical Engineering*, 9(6).

[7] Rostamsowlat I, Akbar B, Evans B. (2018). Analysis of rock cutting process with a blunt PDC cutter under different wear flat inclination angles[J]. *Journal of Petroleum Science and Engineering*, 171, 771-783.

[8] Scott D. (2015). A bit of history: overcoming early setbacks, PDC bits now drill 90%-plus of worldwide footage. In: International Association of Drilling Contractors (IADC) (ed.) *Drilling contractor anthology series—DC drill bits*. Houston, TX: IADC, pp.1–7.

[9] Sun RJ, Ju P, Shi ZJ. (2017). Simulation study of new directional drilling PDC bit used in coal mine[J]. *Geosystem Engineering*, 20(3), 142-148.

[10] Tang QQ, Guo W, Gao K, Gao RF, Zhao Y, Sun Y, Zhou Y.(2018). Design and test of a self-adaptive bionic polycrystalline diamond compact bit inspired by cat claw[J]. *Advances in Mechanical Engineering*, 10(11).

[11] Wang RG, Liao YF, Dai JS. (2019). The isomorphic design and analysis of a novel plane-space polyhedral metamorphic mechanism[J]. *Mechanism and Machine Theory*, 131, 152-171.

[12] Wang SN, Niu QL, Shi BY, Jia W. (2014). Research and computer-aided design of deep-hole PDC reamer bit [J]. *Mineral exploration engineering (rock and soil drilling engineering)*, 41(08), 1-8.

[13] Yang YX, Yang Y, Liu XM, Huang K, Ren HT. (2019). Optimized design and application of a directional reaming-while-drilling polycrystalline diamond compact bit[J]. *Engineering Failure Analysis*, 105, 699-707.

[14] Yang YX, Yang Y, Ren HT, Qi QL, Chen XW. (2020). Research on the working mechanism of the PDC drill bit in compound drilling[J]. *Journal of Petroleum Science and Engineering*, 185.

[15] Yoshida T, Koizumi T, Tsujiuchi N. (2013). Dynamic analysis of an excavator during digging operation. *SAE International Journal of Commercial Vehicles*, 6(2), 419-428.

[16] Zhang JD, Xi FR. (2020). Study on ecological restoration of abandoned mines in China[J]. *Acta Ecologica Sinica*, 40(21), 7921-7930.

[17] Zhu XH, Deng ZL, Liu WJ. (2020). Experimental Study on Energy Consumption of rock cutting under different groove geometry[J]. *Geotechnical Testing Journal*, 43(1), 151-170.